2 Materials Synthesis and Characterizations

2.1 Synthesis of Materials

Pure, monovalent (Na^{+}) and rare earth doped (Ln: $Gd3^{+}$, $La3^{+}$) Strontium cerate (SrCeO3) can be synthesized by a number of ways, each method has its own advantages and disadvantages. The preparative method has been adopted depending on the existing experimental facilities available in the research lab of department. In present work, pure, monovalent and rare earth doped Strontium cerate have been prepared by a simple method called solid state ceramic technique. It is a famous mechanical alloying method which used to synthesize various types of ceramic oxides.

Among the above mentioned doped strontium cerate, lanthanum doped strontium cerate only has been synthesis by auto combustion technique and another by solid state method. Combustion technique is capable of producing ultra-fine powders of oxide ceramics in shorter time and at a lower calcination temperature [161], with improved powder characteristics. The success of this process is due to an intimate blending among the constituents using suitable fuel or complexing agents (e.g. glycine, citric acid, urea and sucrose) in an aqueous medium followed by an exothermic redox reaction between fuel and oxidizer (i.e. Nitrates). Auto ignition, once initiated, is then self-sustaining. The rapid evolution of large volume of gases during the combustion dissipates the heat of combustion and limits the rise of temperature, thus reducing the possibility of premature local partial sintering among the primary particle. It has also been seen that for the synthesis of lanthanum doped strontium cerate by citrate-nitrate auto combustion process, a constant citrate to nitrate ratio (C/N) of 0.4 was observed to be optimum to induce a self-propagating and controlled auto ignition reaction. In the light of these techniques citrate-nitrate auto combustion method is relatively simple and cheap process to synthesize nano-size powder.

After synthesis of the compound, each of the prepared compounds needs to be characterized to evaluate their structural and physical properties and their applications. To

explain the basic Physics involved in each system, the characterization part is important. The calcination temperature i.e., temperature at which the reaction among the raw materials took place for the prepared mixture is determined using Thermogravimetric (TG) and Differential scanning calorimetry (DSC) analysis. Structural and microstructural characterizations of all examined samples are studied by a powder X-ray diffractometer (XRD), Scanning electron microscope (SEM) and Transmission electron microscope (TEM). Raman Spectroscopy and Fourier transform infrared (FTIR) spectroscopy studied the presence of the rotational, vibrational band and various functional groups. The compositional analysis of samples is carried out using Energy Dispersive X-ray (EDX) spectrometer attached to SEM facility and X-ray photoelectron spectroscopy (XPS). The absorption of the prepared compositions is measured by an Ultraviolet-Visible (UV-Vis) spectrometer, and its optical band gap is determined using a well-defined Tauc's relation [162]. The electrical properties of prepared compositions are investigated using a high precision LCR meter.

The details of preparative methods, experimental techniques and the basic working principle of the instruments used are summarized and presented subsequently in this chapter.

2.1.1 Mechanical Alloying Method

In the late 1960s, Benjamin, his co-workers and their International Nickel company were the first to developed the cost-effective and less time engrossing mechanical alloying process for sample's preparation. This method became more acceptable among the researchers to prepare the new phase and structure of oxide materials in the late 1900s. The energy generated in this process through high speed rotation of ball inside the pot. The mixture of desired compositions has been prepared from the commercially available raw materials. This process is also known as high energy ball milling, widely accepted for the preparation of nanomaterial of various ceramic oxides. It is a well-controlled preparative technique by which

new compounds, new structure, and phases can be formed through activating and calcining of the starting materials.

In this method, the powder precursors are kept inside the tightly closed vial with balls made up of the same material as that of the vial. The vials are rotated with a predefined rotation speed for some particular duration. The formation of new phases and compounds took place by the mixing of precursor powder. The precursor powder subsequently underwent several processes such as fractured, welded and activated processes and finally formed and collected the Nano powders from the vials. Selectivity of the material of vials and balls depended on the nature of chemical used in sample preparation so that the precursors did not react chemically with the vial and balls. The conventional materials for vials and balls are Stainless steel, zirconia dioxide, tungsten carbide, etc.

2.1.1.1 Mechanism of Ball-Mill

The mechanism of a planetary ball mill is shown in **Figure 2.1**. The grinding action was strictly depending on the rate and intensity of the collision of the balls with the sample, which depends on the rotation speed of disc (**Ω**), vials around itself (**ω**), radius of disc (***R***) and vials (***r***), mass or weight of the ball (***m***) and number of balls (***n***). The formation of end products in planetary ball mill barely depends on the shock power and the power transferred to the powder in each collision by the ball. The power (P) is given by the mathematical formula;

$$P \propto ml^2\Omega^2 \tag{2.1}$$

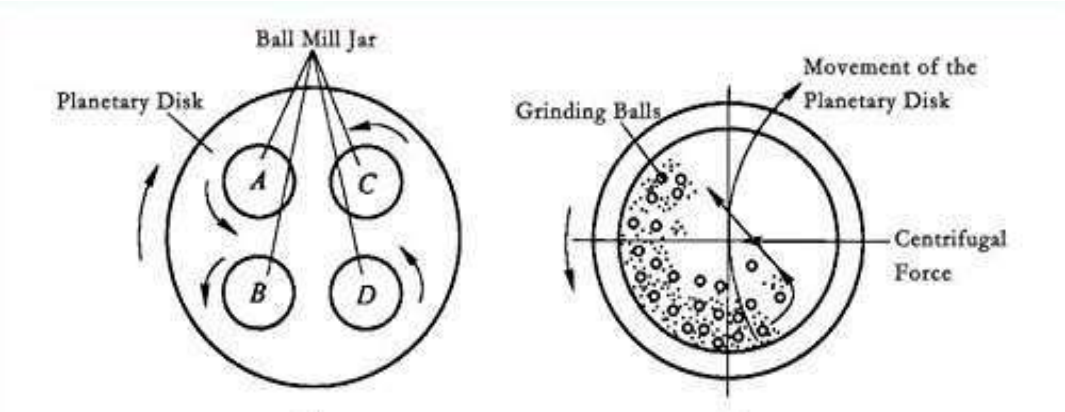

Figure 2.1 Working Principle of Lab Planetary Ball-Miller.

Where, l^2 is the characteristic area. The precursor of raw materials is converted into the fine powder by the shock power generated between collisions of the balls with the inner wall of the closed vial through a number of steps. Initially in the mixing process the powder gets mixed then fragmented afterward coalesced and finally the phase transformation and amorphization takes place. The nature of final product depends on the milling conditions such as milling atmosphere, initial powder composition, balls to powder mass ratio, the materials of balls and vial, average milling time and temperature generated by the milling process.

Advantages

I. Low-cost installation and grinding medium.

II. One pot, one step mechanosynthesis.

III. Fabrication of materials at room temperature.

IV. Revolution per minute (rpm) and milling time can be programmed for user-defined.

V. Suitability of choosing milling atmosphere.

VI. Applicable to materials having all degree of hardness.

VII. Synthesis of a new phase is possible with localized deformation.

VIII. Formation of particles in the nano dimension or even in the amorphous phase and also controls the particle size of final product.

IX. Formation of a complete solid solution.

X. Complex powder formation in a concise time.

XI. Various milling parameters can control shock energy.

Disadvantages

I. Contamination from the milling medium.

II. Stickiness of the sample with container results loss of materials.

III. Excessive heating during milling.

The optimisation of milling parameters overcomes by minimizing above mentioned disadvantages. The duration of milling time has to be optimized time to time and sample to sample to avoid contamination from the milling medium. The excess heat generated from the milling can be controlled by controlling the rpm of the vials. The balls to powder mass ratio (BPMR) and the milling atmosphere are chosen to ensure the purity of the final product.

2.1.2 Citrate-Nitrate Auto-Combustion Method

Self-propagating high temperature synthesis also known as auto combustion is an important technique widely used for the synthesis of a variety of metal nitrates for different applications. This method has some advantages over other methods like solid state reaction method, sol-gel process, ultrasonic spray pyrolysis technique etc. which is given below

(1) The required reagents are simple compounds,

(2) There is no need for special equipment,

(3) Dopants can be easily introduced into the final product,

(4) An agglomeration of powders remains limited,

(5) 20-50 nm size nanoparticles can synthesize,

(6) Less time and least cost process and

(7) Neither inert gas nor vacuum is required

In the combustion mixture, nitrates and organic compounds behave like conventional oxidants and fuels. First La $(NO_3)_3.6H_2O$ (lanthanum nitrate) was dissolved in distilled water with other nitrate solutions to get the homogenous mixture. Ammonia solution was used to achieve a particular pH value for proper combustion. The value of the pH is maintained at 6 to avoid phase segregation and to provide a true homogeneous distribution of all the cations at the atomic level. The solution formed with all precursors was heated to evaporate water on a hot plate in the temperature range 160-200ºC with the help of magnetic stirrer bar which gave thick gel. The formed gel slowly foamed, swelled, and finally burnt on its own on a hot plate. The dark gray voluminous power (ash) was formed within few seconds. Exothermicity of combustion is controlled by the nature of the fuel and the ratio of oxidizer to fuel. Then the aqueous solution of citric acid was added to keep citrate-nitrate ratio (C/N) equal to 0.4. As prepared ash was grounded in an agate mortar and calcined in a crucible at 1000 °C (as per DTA and TGA curve) for 10 hours with a heating rate of 5 °C/min. This powder was grounded and pressed uniaxially under an optimum load of 7 kg/m^2 to form cylindrical pellets having a thickness in the range 1-2 mm and diameter 12 mm using a hydraulic press. For sintering, pellets were kept in a platinum crucible, covered with a platinum lid. These pellets were sintered at 1200 °C for 12 hours in the air. Thereafter, the temperature was raised to a required sintering temperature at a rate of 5 °C/min, kept at this temperature for a required soaking period and then cooled to room temperature at a rate of 5 °C/min. A flow chart of auto combustion synthesis techniques is shown in the **Figure 2.2**.

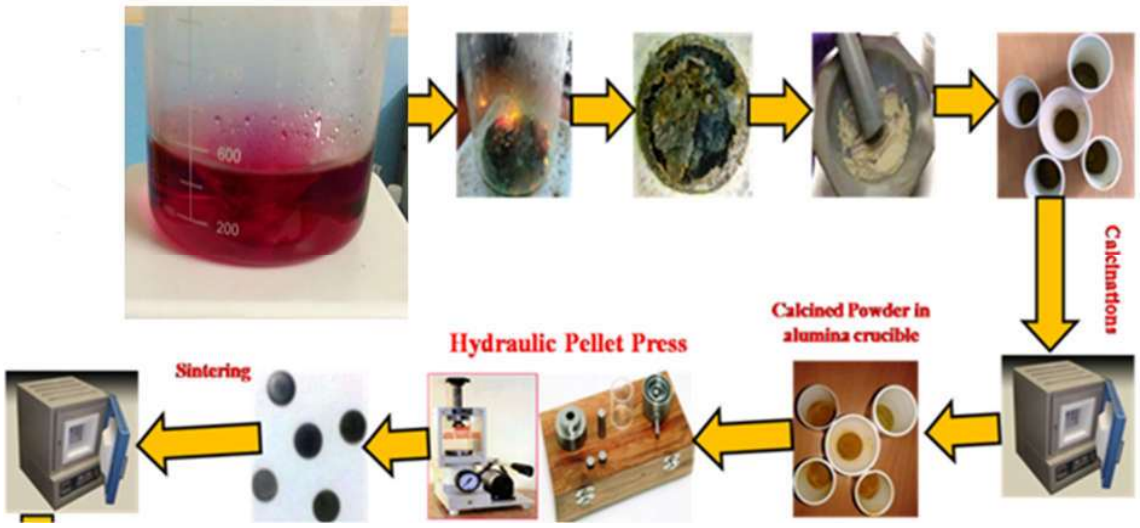

Figure 2.2 Flow chart of auto combustion synthesis.

2.1.3 Raw Materials

High purity raw materials of these investigated compositions were used for synthesis process by solid state ceramic route by ball milling and auto combustion in the thesis work. The specifications of these materials are listed in Table 2.1. The schematic representation of the methodology for sample preparation is shown in **Figure 2.3**.

Table 2.1 Specification of materials used in synthesis.

Raw Materials	**Purity**	**Manufacturer**
$SrCO_3$	99.99%	Alfa-aesar, USA
CeO_2	99.99%	Alfa-aesar, USA
$Na_2CO_3.H_2O$	99.99%	Alfa-aesar, USA
Gd_2O_3	99.99%	Alfa-aesar, USA
$La(NO_3)_2H_2O$	99.99%	Alfa-aesar, USA
$Sr(NO_3)_2$	99.00%	Alfa-aesar, USA
$(NH_4)_2Ce(NO_3)_6$	99.50%	Alfa-aesar, USA

Figure 2.3 Schematic representation of mechanical alloying method.

2.1.4 Preparation of Materials using Ball Milling

In this thesis work, a vial is made up of chrome steel (The inside layer is coated with Zirconia) was simultaneously rotated with 5 zirconia balls each of 10 mm diameter kept inside the tightly closed steel vial. A stoichiometric amount of raw materials as shown in Table 2.1 are taken in a 100 ml chrome steel vial, partially filled with zirconia balls in the ratio of 1:40 balls to mass ratio. The closed steel vial is then mounted on a planetary ball mill (PM 200, Retsch, Germany) and rotated with the speed of 200 rpm for 8 h with intermediate pauses. The high speed creates an impact between the balls and sample which is generated by the centrifugal force between the balls and inner-wall of the vial. The samples are kept with balls inside the vial to help grinding sample homogeneously. Finally, the milled powder is transferred to alumina crucible from the vial and subsequently dried in an oven for 24 h at 60 ºC. Subsequently dried powders have transferred to agate mortar and then grounded again for homogeneity.

2.1.5 Calcination of Materials

The heating of a solid to a high temperature below its melting point which creates a condition for thermal decomposition or phase transition in or other than melting or fusion termed as calcination. In order to know the calcination temperature of obtained powder, the thermal analysis (TG/DSC) of prepared mixture was performed. In addition to that, the obtained mixture was transferred to an alumina crucible and put inside the programmable muffle furnace and heated to 1100 ºC for 12 h to obtain single phase powder. After the successful preparation desired compositions were subjected to various other characterization techniques as discussed in the subsequent section.

2.1.6 Granulation and pelletizations

The obtained powder after calcination was uniformly mixed using pestle in an agate mortar. Afterward, 2 % polyvinyl alcohol (PVA) was uniformly then mixed into powder until it become fine. The obtained fine powder was then pelletized using a hydraulic press with the help of a die having 10 mm diameter by applying the pressure of 7 kN. The obtained pellets are then used for the further characterization.

2.1.7 Sintering

Sintering is the process of heating for microstructural change, densification and crystal growth of the material. Sintering of the materials has carried out in several steps of thermal heating. The furnace was heated to 200 ºC at a heating rate of 2 ºC /min, kept at this temperature for 1 h to burn off binder completely. Then pellets were further heated to 1200 ºC at a heating rate of 5 ºC /min and soaked at this temperature for 12 h for sintering process. The pellets were then cooled to 600oC at a rate of 5 ºC /min and thereafter with normal cooling rate to the room temperature. The further characterization techniques to study the phase formation, microstructure and electrical properties of pellets were carried out and described in subsequent section.

2.2 Materials Characterization

2.2.1 Thermal analysis (TGA-DSC)

The thermo-gravimetric analysis (TGA) is a technique which is used to determine the calcination temperature of the sample and also used to evaluate the stability of materials. In this analysis, the change in mass of the experimental sample has been recorded as a function of temperature which provides the information about the mass gain (absorption), mass loss (desorption), phase transition, etc. of the sample [163]. If the mass of the sample remains constant in a given temperature range, then the sample is said to be thermally stable within that temperature range. TGA also provides information about the upper limit of temperature beyond which the sample starts degrading. In literature, TGA is widely used to know about the reaction temperature of the sample, stability of materials, etc.[90].

Differential scanning calorimetry (DSC), measures the change of the difference in heat-flow rate of the sample to the reference sample when subjected to a controlled temperature program. The sample of known mass is heated or cooled and during this process, the change in heat capacity is recorded in terms of changes in heat flow. Using this technique, the type of reaction (Endothermic or Exothermic), enthalpy, Gibbs energy and other thermal parameters are derived. The combined study of TGA-DSC also gives an idea about the reaction pathway for the prepared mixture of raw materials and various transition points such as melting point, glass transition temperature, crystallization temperature, etc. In present thesis work, the TGA-DSC measurement was carried out by TGA/DSC (Mettler Toledo, Germany) model, operated within the temperature range from 27 ºC -1000 ºC in the presence of nitrogen gas atmosphere.

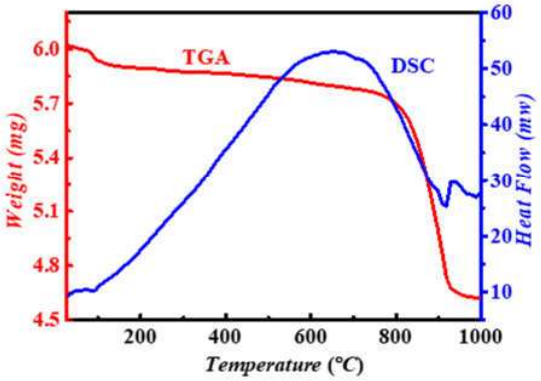

Figure 2.4 TGA-DSC facility. **Figure 2.5** A typical non-isothermal TGA-DSC Curve

2.2.2 Measurement of Density and Porosity

The density (ρ) of prepared samples was calculated using Archimedes principle. For this purpose, the pellets of each coposition were made. The powders of each composition were mixed with 2% polyvinyl alcohol (PVA) and pelletized with the help of vertical die having diameter 10 mm and thickness 2 mm on application of a normalized load of 6 Ton by Hydraulic press. In this method first pellets are weighed in air, later on the pellets are immersed into the immersion liquid. Acetone ($\rho_{ace} = 0.79 gcm^{-3}$) was used as immersion liquid for present thesis work. Let m_{dry} and m_{ace} are the weight of pellet in air and acetone medium respectively, then the actual density of the sample is given by

$$\rho = \frac{\rho_{ace} * m_{dry}}{m_{dry} \sim m_{ace}} \tag{2.2}$$

In the present thesis work, two different pellets of each composition were weighed three times and their average value is taken as the experimental density of the sample. The weighing measurement was performed using a digital balance having an accuracy of ±0.00001 gm. as shown in **Figure 2.6**.

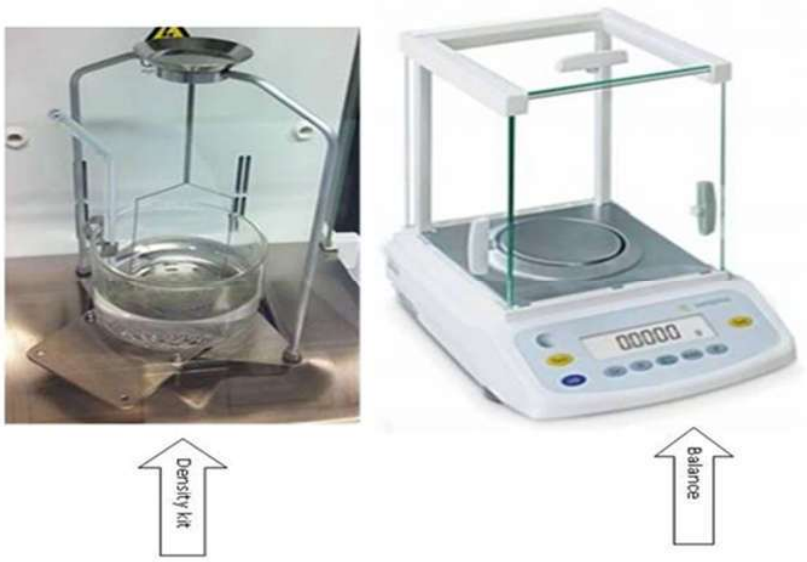

Figure 2.6 Balance with density kit [Sartorius, BSA2245CW]

Theoretical density was determined from the molecular weight of the compound and lattice parameters using the relation,

$$D_{th} = \frac{n \times M}{N \times V} \tag{2.3}$$

Where, D_{th}, n, M, N and V are theoretical density, number of formula unit per unit cell, molecular weight of the sample, Avogadro's Number and unit cell volume respectively. Percentage porosity was calculated using the relation

$$\%\ porosity = \left(\frac{D_{th} - D_{exp}}{D_{th}}\right) \times 100 \tag{2.4}$$

2.2.3 Phase Formation and Crystal Structure Studies by Powder X- ray Diffraction

The powder X-ray diffraction (XRD) is a versatile and an essential characterization technique for phase identification which has been established over the years. The name powder X-ray diffraction is associated with the technique which connects XRD pattern from a packed powder specimen. The powder samples are made up of many microscopic polycrystals, randomly oriented domains in all possible directions, resulting in the XRD pattern. The domain which gives diffraction in the same direction is known as coherently diffracting domains. This

technique is used to determine the crystal structure, preferred orientation of lattice planes, crystallite size, shape and size distribution of polycrystalline powder [164]. It is a non-destructive technique in which the samples can also be exposed to different pressure and temperature conditions during collection of the diffraction pattern.

2.2.3.1 Bragg's law

The X-ray diffraction (XRD) method follows Bragg's law of X-ray diffraction. This law can be obtained geometrically, as depicted in **Figure 2.7**.

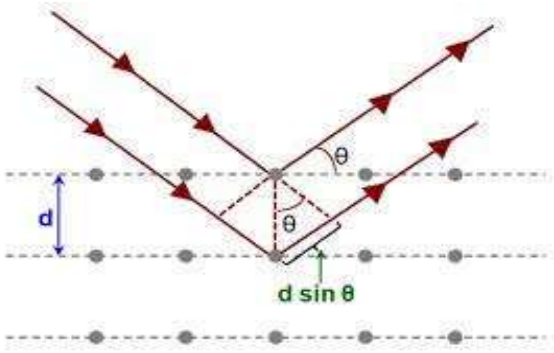

Figure 2.7 Visualization of Bragg's law.

Consider a set of crystallographic lattice planes with an interplanar spacing $d_{hkl}$is irradiated by a plane wave X-ray. Let θ be the angle of incidence between X-ray beam and lattice plane, the interplanar spacing d_{hkl} creates a path difference for the ray scattered from the top & bottom surface of the plane. Using the geometry, the path difference between incident and diffracted ray is found to be $2d_{hkl}Sin\theta$. If the path difference is an integral multiple of wavelength (λ), then the interference between the scattered rays can be said to be constructive. Mathematically Bragg's law is given as:

$$2d_{hkl} \sin\theta = n\lambda \tag{2.5}$$

Where, n is an integer and said to be an order of diffraction.

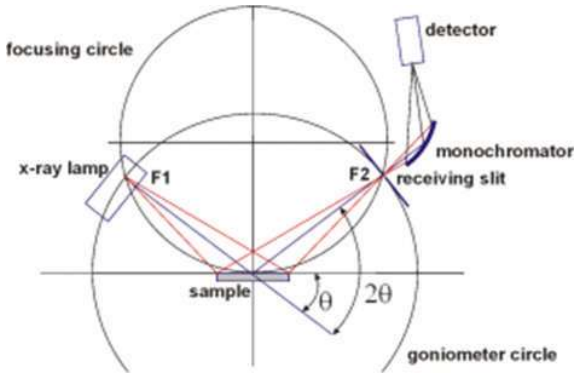

Figure 2.8 Schematic representation of $\boldsymbol{\theta/2\theta}$ diffraction in Bragg-Brentano geometry.

The basic geometry used in most of the X-ray diffractometer is shown in **Figure 2.8**. The angle of the incident ray and scattered ray with respect to the specimen surface is θ. The XRD pattern is recorded by varying the incident angle of X-ray beam by θ angle and the scattering angle by 2θ. Finally, the scattered intensity (I) has recorded as the function of 2θ. In some cases, the X-ray source remains stationary while the sample is rotated by angle θ and the detector moves by 2θ. Moreover, in most of the cases, the sample is fixed while both the X-ray source and the detector simultaneously rotated by angle θ. Such precise rotation in the diffractometer is performed by goniometer which is the central part of the diffractometer. Typically, the sample is mounted on the rotational axis, the X-ray source and detector move along the periphery.

The Rietveld refinement analysis of the powder XRD pattern from a polycrystalline sample has been performed on well resolvable diffraction data. For this purpose, the XRD data were recorded in step scan mode with a slow scanning rate. The different crystallographic phases of the present sample were extracted by recording X-ray diffraction pattern at room temperature using, X-ray diffractometer (Rigaku Miniflex II, Japan) equipped with Cu Kα radiation having wavelength λ=1.5418 Å at an applied voltage of 40 kV and current 40 mA. The XRD pattern

has been recorded in the angular range of 20 °-80 ° with step size 0.02 ° and scan @ 0.02 °/min. We have used the width of the primary divergence slit was 0.6 mm, and for the secondary detector, the slit was at 1.0 mm for X-ray diffraction measurements. The X-ray diffractometer used for present thesis work is shown in **Figure 2.9**.

Figure 2.9 XRD facilities, Central Instrument Facility (CIF) IIT (BHU).

2.2.3.2 Phase Matching

In the powder XRD pattern, the peaks are generated from the randomly oriented planes identified by the respective Miller indices (hkl). The XRD peaks are indexed and matched by standard phase identification method which contained Miller indices, relative intensity with similar interplanar spacing or diffraction angles and other crystallographic information [165.]. The standard database is maintained by "**International Center for Diffraction Data (ICDD)**" formerly known as the "**Joint Committee for Powder Diffraction Standards (JCPDS)**." There is another database available freely for users named as "**Crystallographic Open Database (COD)**." In present thesis work, the experimental XRD pattern is matched with the COD database. Another alternative method besides this search match method is the simulation method in which the theoretical XRD pattern is generated by computer program through structural information available from the ICDD database. This method is only applicable when

the crystal phase(s) or similar structure file is available in the ICDD database. The gross computed XRD pattern is then refined to fit the experimental XRD pattern by modifying several instrumental, structural and microstructural parameters through the continuous iteration process [166].

2.2.3.3 Rietveld Refinement Study

The Rietveld method is proposed in International Union of Crystallography (IUCr) stated as "Method of analysing powder diffraction data in which the crystal structure is defined by fitting the entire profile of the diffraction pattern to a calculated profile using a least-square approach. There is no intermediate step of extracting structure factors and so patterns containing many overlapping Bragg peaks can be analysed" [166]. The obtained experimental XRD pattern is undergone through identification of crystalline phases(s) matched with the available materials in the COD database. After the phase identification, individual detailed structure file so-called crystallographic information file (CIF) is taken for further process. A theoretical XRD pattern is simulated by Rietveld refinement software using CIF file. In order to study about the structural and microstructural characterizations following information must be provided **(a)** instrumental correction factor like peak shift, peak broadening and asymmetry in peak **(b)** approximate value of crystallite size and lattice strain. The experimental XRD pattern is refined by simulated XRD pattern through iterative method keeping another parameter as constant to obtain the structural and microstructural parameters. The Marquardt least square fitting method has been used in the present case. The best fit between intensities of simulated and experimental XRD pattern is achieved by successive refinement of structural and microstructural parameters until the parameters are converged. The quantity S_y is minimized through least square method defined as-

$$S_y = \sum_i W_i (I_{oi} - I_{ci})^2 \quad (2.6)$$

Here, $W_i = 1/I_{oi}$, I_{oi} = observed intensity at i^{th} step and I_{ci} = calculated intensity at i^{th} step. The best fit is achieved when S_y attains a minimum value. The value of I_{ci} is obtained by summation of all calculated intensities and background contribution given by

$$I_{ci} = S \sum_k L_k |F_k|^2 \emptyset(2\theta_i - 2\theta_k) P_k A + I_{bi} \quad (2.7)$$

Here, S is the scale factor, L_k contains Lorentz polarization factor and multiplicative factor, k represents Miller indices hkl for a Bragg reflection, F_k is the structure for k^{th} Bragg reflection, $\emptyset$ is a reflection profile function which approximate the effect of aberration due to absorption, specimen displacement, crystallite size, microstrain etc., P_k is the preferred orientation function, A is an absorption factor, I_{bi} is the background intensity of i^{th} step, $2\theta_k$ is the diffraction angle of k^{th} Bragg reflection.

The Rietveld refinement of X-ray diffraction pattern is a critical process because it requires many calculations due to the involvement of many parameters. For that purpose, sophisticated software is required which correlate the calculated and experimental XRD pattern at each step and so that software should be user-friendly. There is some Rietveld software is available free of cost and are being used by many users worldwide, FullProf software package has been used in present thesis work for Rietveld refinement purpose.

Rietveld refinement software is applied on the X-ray powder diffraction data developed by H.M. Rietveld in 1969 [167]. This software package is also used as a profile matching tool without knowledge of the crystal structure. This software is capable of evaluating the various structural and microstructural parameters with the incorporation of all recent development. A typical interface of FullProf software is shown in **Figure 2.10**. This software is used to analyze X-ray diffraction of different samples from bulk to nano dimension.

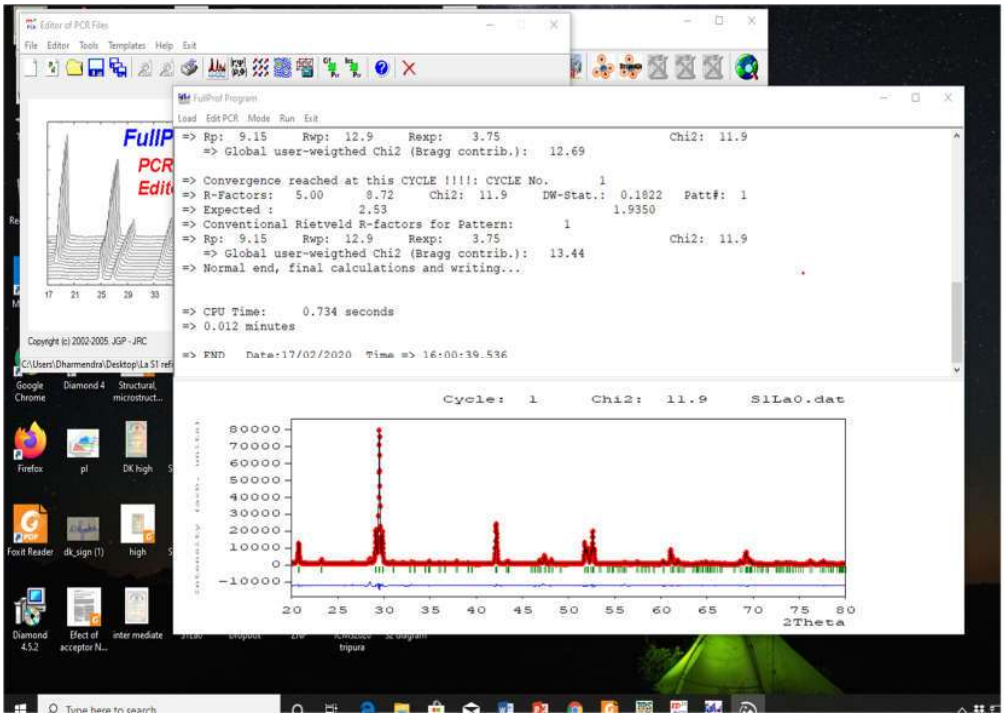

Figure 2.10 A typical FullProf software interface during Rietveld refinement process.

The main features and advantage of FullProf software are-

1. The X-ray diffraction data, collected by Laboratory set-up and synchrotron sources and neutron diffraction sources can be used for refinement through this software.
2. The backgrounds are defined by a variety of function like constant function, higher order polynomial through Fourier filtering.
3. The peak shape is modelled in variety of functions for each phase: Gaussian, Lorentzian, modified Lorentzian, pseudo-Voigt, Pearson-VII, Thompson-Cox-Hashing (TCH) pseudo-Voigt, numerical, split pseudo-Voigt, the convolution of a double exponential with a TCH pseudo-Voigt.
4. The Rietveld refinement can be performed for multiple phases (up to 16 phases).
5. Two types of functions are available for the modelling of preferred orientation of peak.

6. Absorption corrections for different geometries and micro-absorption correction for Bragg-Brentano set-up are available.
7. It provides the choice of automatic generation of hkl and/or symmetry operators.
8. Magnetic structure refinement can also be performed.
9. Automatic generation of reflections for an incommensurate structure up to 24 propagation vectors.
10. hkl dependence of the position shifts of Bragg reflections for special kind of defects.
11. Quantitative analysis has been performed without the need for structure factor calculations.
12. The instrumental resolution function (Voigt function) may be supplied in a file then the microstructural analysis is then performed.
13. Popa-Balzer model can add anisotropic crystallite size and strain.
14. For a better view of the simulated pattern along with the experimental pattern, the square root of intensity is plotted against 2θ.

The quantitative measure of different phases present in a multiphase compound directly depends on the scale factor of Rietveld refinement [168]. For a multiphase system with known molecular weight, the weight fraction phase can be calculated using the relation

$$W_i = \frac{S_i(ZMV)_i}{\sum_j S_j(ZMV)_j} \tag{2.8}$$

Here, S_i is the scale factor, Z_i is the number of molecules per unit cell, M_i is the molecular weight and V_i is the unit cell volume of i^{th} phase present. The density of i^{th} phase can be evaluated using the following relation-

$$\rho_i = \frac{Z_i M_i}{N_A V_i} \tag{2.9}$$

N_A is Avogadro number. It is important to calculate the relative phase abundances in a multiphase compound for its different scientific and industrial applications. Rietveld analysis

was found to be a very successful method to determine the phase fraction of multiphase material. X-ray diffraction profile fitting by Rietveld refinement method utilizes the minimization of different structural and microstructural parameters by an iterative method [37]. These methods refine and adjust different parameters until the residue between experimental intensities (I_{oi}) and calculated intensities (I_ci) is minimized. Following residue parameters are used to define the quality of fitting.

The residue of structure factor

$$R_F = \frac{\sum_i |\sqrt{I_{oi}} - \sqrt{I_{ci}}|}{\sum_i |\sqrt{I_{oi}}|} \tag{2.10}$$

The residue of Bragg factor

$$R_B = \frac{\sum_i |I_{oi} - I_{ci}|}{\sum_i |I_{oi}|} \tag{2.11}$$

The residue of weighted pattern

$$R_{wp} = \left| \frac{\sum_i W_i (I_{oi} - I_{ci})^2}{\sum_i W_i (I_{oi})^2} \right|^{\frac{1}{2}} \tag{2.12}$$

The residue of expected pattern

$$R_{exp} = \left| \frac{N - P}{\sum_i W_i (I_{oi})^2} \right| \tag{2.13}$$

In all the equation I_i is the intensity of i^{th} Bragg reflection at the end of the refinement, the letter o and i in suffix represents the observed and calculated intensities. W_i and N represents the weight and number of experimental observation and P represents the number of refineable parameters. The refinement process has been continued till convergence of this parameter is reached. The quality of fit is also monitored by "Goodness of fit" (GOF) defined as

$$GOF = \frac{R_{wp}}{R_{exp}} \tag{2.14}$$

For best fit, the GOF is approx. 1.00 which means the calculate pattern fully matched with the experimental pattern.

2.2.3.4 Size-Strain Analysis

The microstructural analysis of a polycrystalline compounds has been studied in terms of crystallite (particle) size, lattice strain and imperfections (dislocations and stacking faults) by analysing the XRD pattern by following methods: **(a)** The integral width method (Williamson-Hall plot) **(b)** The Variance method **(c)** Fourier Transformation Method (Warren-Averbach line profile analysis). Practically, no polycrystalline sample is ideal so that the diffraction peaks are broadened with finite peak width. The broadening in XRD peaks is appeared due to **(a)** Instrumental broadening **(b)** Small crystallite size **(c)** Accumulation of lattice strain **(d)** Presence of different kinds of stacking faults in the lattice.

The analysis of diffraction pattern by integral breadth method can predict the finite particle size and microstructure of the composition. Scherer introduced this method in 1918 and Stokes and Wilson further modified it [169]. This is the oldest method widely used for determination of particle size and strain. In this method, the width of diffraction line is defined as the angular width of the peak in radians at a point where the intensity reduces to half of its highest value, i.e., full width at half maxima (FWHM). Max-Von Laue proposed another method to measure the breadth of diffraction peak as:

$$\beta = \frac{1}{I_p}\int I(2\theta)d(2\theta) \tag{2.15}$$

Here, β is integral width, I_p is the peak intensity and $I(2\theta)$ is intensity at diffraction angle 2θ. In 1949, Hall suggested the integral breadth should be described as the summation of two broadening given by (After correction of instrumental broadening and neglecting broadening due to lattice imperfections).

$$\beta = \beta_D + \beta_S \tag{2.16}$$

Here, β_D and β_S are peak broadening due to small crystallite size and microstrain in lattice respectively. The β_D is measured by Scherrer equation-

$$\beta_D = \frac{k\lambda}{DCos\theta} \tag{2.17}$$

Where λ is X-ray wavelength, k is the crystallite shape constant ($k = 0.89$ for spherical shape), D is the crystallite size and θ is the Bragg angle. β_S is the broadening arising from the microstrain in the compound given by

$$\beta_S = 4\epsilon\, tan\theta \tag{2.18}$$

Where ϵ is the microstrain in the lattice, so **Eq (2.15)** can be rewritten as

$$\beta = \beta_D + \beta_S = \frac{k\lambda}{DCos\theta} + 4\epsilon\, tan\theta \tag{2.19}$$

$$\frac{\beta Cos\theta}{\lambda} = \frac{1}{D} + \frac{4\epsilon Sin\theta}{\lambda} \tag{2.20}$$

Thus by measuring the FWHM (β) and corresponding Bragg angle of all reflection appeared in the XRD pattern of the polycrystalline sample. A straight line (best fit) using **Eq (2.19)** obtained by plotting the curve between $\frac{\beta Cos\theta}{\lambda}$ along ordinate and $\frac{Sin\theta}{\lambda}$ along abscissa is known as Williamson-Hall Plot. The intercept of the straight line on ordinate gives the measure of $\frac{1}{D}$ and slope of the straight line gives the measure of average microstrain (ϵ).

In Williamson-Hall plot the line broadening in XRD peaks is primarily considered to be isotropic. This indicates that the diffracting domains were isotropic and microstrain contribution was also present. However, in the case of isotropic line broadening, a better evaluation of size-strain parameters was obtained by "Size-Strain plot (SSP)" method. The advantage of this method is that less weightage has been given to the data obtained at high angles, where the prerecession is usually lower. In this approximation, the crystallite size profile is considered to be a Lorentzian function and the strain profile by a Gaussian function [170]. Accordingly, we have

$$\left(\frac{d_{hkl}\beta cos\theta}{\lambda}\right)^2 = \frac{k\lambda}{D}\left(\frac{{d_{hkl}}^2\beta cos\theta}{\lambda^2}\right) + \left(\frac{\varepsilon}{2}\right)^2 \tag{2.21}$$

Where d_{hkl} is the interplanar spacing corresponding to the plane (hkl), ε is the average strain produced in the lattice, k is a constant which depends on the shape of particles, for example, it is ¾ for a spherical particle. Similar to the W-H plot, the term $\left(\frac{d_{hkl}\beta cos\theta}{\lambda}\right)^2$ plotted with respect to $\left(\frac{{d_{hkl}}^2\beta cos\theta}{\lambda^2}\right)$ for all diffraction peaks. The particle size was determined from the slope of the linearly fitted data while the square root of the intercept gives the strain.

2.2.4 Raman Spectroscopy

Raman spectroscopy is an analytical tool concerned with radiation scattering from a sample such that the structural parameters at the local level can be studied based on vibrational transition within the materials. In Raman spectroscopy, incident laser beam interacts with molecules to produce characteristics pattern and when a small fraction of incident laser radiation is scattered by the molecule and then it brings difference in wavelength from the incident beam. The shifts in wavelength depend on the chemical structure of molecules responsible for the scattering. The molecule experiences a momentary distortion of electrons, distributed around a bond by the incoming photon from the laser which creates an induced dipole moment in the molecule followed by re-emission of photon when it relaxes. When the molecule relaxes, the frequency of some photons is changed (Raman Scattering) and do not return to their original state and shifted to a new energy state which is known as Raman Shift [171]. Raman shift can be treated as fingerprint of the materials. The Raman spectra of the samples investigated in thesis work were recorded by a Jobin Yvon Horiba T64000 system equipped with a TE-cooled charge coupled device detector and an Olympus microscope using He-Ne laser of wavelength 632.817 nm used as the excitation source in wavenumber range 100-1000 cm-1 as shown in **Figure 2.11**.

Figure 2.11 Experimental set-up used for Raman Measurement (CRF IIT Kharagpur).

The working principle of a Raman spectrometer has been described as shown in **Figure 2.12** which consist of four major components: **(a)** Excitation source (LASER) **(b)** Sample illumination system **(c)** Light collecting optics, wavelength selector (Filter, spectrophotometer) **(d)** Detector (Photodiode array, CCD or Photo-multiplier-tube(PMT)). The sample is generally illuminated with a laser beam of ultra-violet (UV) or visible (Vis) or near-infrared (NIR) range as available with a spectrometer and the scattered light sent through interference filter is collected by a lens to Raman spectrometer and recorded the Raman spectrum of the investigating samples. Raman spectrum is an invaluable analytical tool which provides information about molecular fingerprint as well as it monitors changes in molecular band structure (e.g. state changes and stress & strain). The light coming from excitation laser source interacted with the molecular vibrations, phonons or other excitations present in the system under investigation, the resulting energy of the laser photons being shifted in either up or down direction. The energy shifts in materials called as Raman Shift, shift in the energy towards higher band known as Anti-Stokes while shift in energy towards lower band known as Stokes

Raman scattering respectively, thus providing information about the vibrational modes of the system.

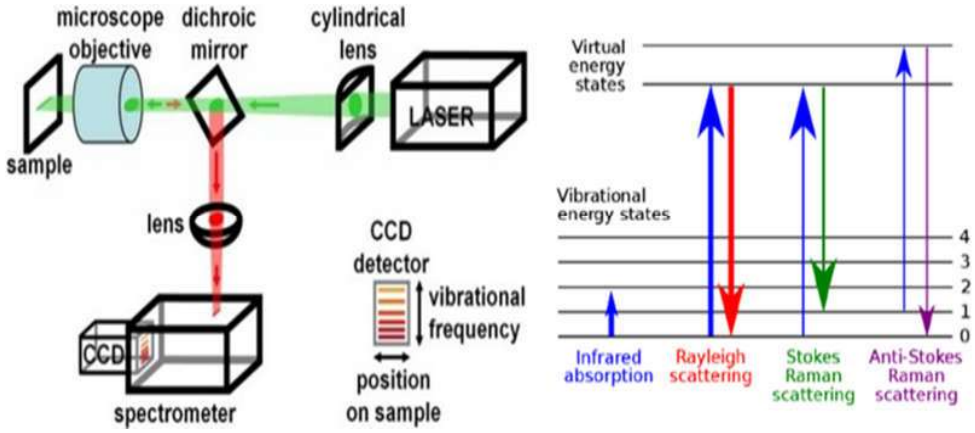

Figure 2.12 Schematic presentation of the principle of Raman Spectroscopy

2.2.5 Fourier Transform Infrared Spectroscopy (FTIR)

Infrared spectroscopy is an important technique for analysis of materials also provides the fingerprint of the samples investigating in this work. The absorption of FTIR peaks corresponding to the frequencies of vibrations between the bonds of the atom which is responsible for building up the materials. Since each material possesses a unique combination of atoms and no two compounds produce the exactly same infrared spectrum. Thus IR spectroscopy can provide identification (qualitative analysis) of different kinds of materials [171]. A schematic diagram of Fourier transforms infrared (FTIR) spectroscopy is shown in Figure 2.13. The FTIR is preferred over other infrared spectrum analysis due to following reasons

- It is a non-destructive technique.
- It provides a precise measurement method which requires no external calibration.
- It can increase the speed of data collection and scan every second.

- It has greater optical throughput.
- It is mechanically simple with only one moving part.

In this thesis work, the FTIR spectra of the powdered samples in transmission mode were recorded by an FTIR spectrophotometer of Shimadzu; model DF 803 Japan as shown in **Figure 2.13** by taking sample to KBr in 1:100 mass ratios within wavenumber range 400-4000 cm-1 at room temperature.

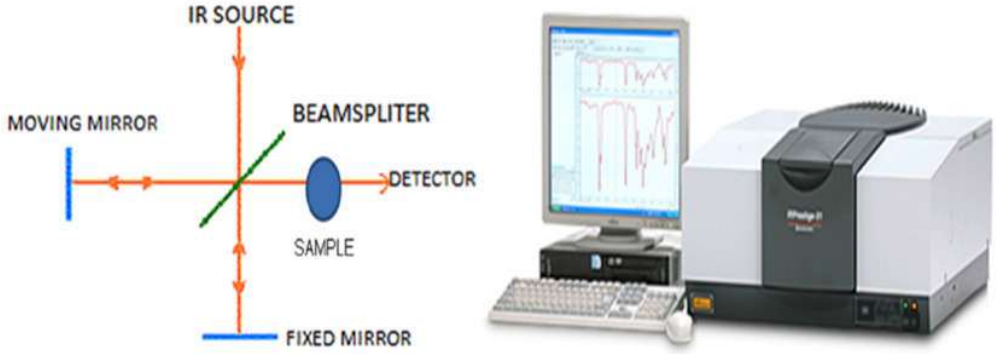

Figure 2.13 Principle of FT-IR spectroscopy and experimental set-up for FTIR measurement facility.

2.2.6 Microstructure and Elemental Analysis

2.2.6.1 Transmission Electron Microscopy (TEM)

Transmission Electron Microscopy (TEM) is one of the most powerful technique to characterize materials with a nano-meter scale feature [172]. The TEM was firstly built by Max Knoll and Ernst Ruska in 1931 while the first experiment at TEM was performed on resolution higher than an optical microscope in 1933. In view of the small de-Broglie wavelength of the electron, TEM is capable for imaging the specimen at resolution of atomic level. TEM has been used for the multiple imaging modes that extend the examination of specimen from the various aspects. **(a)** Bright field TEM images are generated directly by the transmission of electrons. Under this mode of imaging size, shape, uniformity and disparity of nanomaterials can be

directly observed. **(b)** Dark field TEM allows one to use diffracted electron from a specific set of crystal planes to imaging of the materials and often used to locate defects in crystals. **(c)** High-resolution TEM (HR-TEM) has been extensively used to study the lattice structure of crystals. It is very useful in discovering the crystalline nature and crystal defects present in the sample like stacking fault, twinning of nanomaterials.

Transmission electron microscopy is an excellent microanalysis technique to analyze for atomic structure of the sample and thus it needs a meticulous sample preparation. The morphology of nanomaterials is the basic study in the present thesis work and for this purpose the HR-TEM has been recorded and analysed. First the samples were ground in mortar pestle; thereafter a pinch of powder samples was dispersed ultrasonically in a minimal amount of isopropyl alcohol for 2 h. Then a small drop of solution was placed on a carbon-coated Cu grid (300 meshes). The copper grid was dried in an oven for overnight in the vacuum of 10^{-6} bar pressure. The dried grid was taken for the electron microscopy measurement in grid holder. When a high energy electron beam generated by electron gun falls on the sample mounted in the specimen stage after passing through the condenser lens system. A number of incidents take place due to elastic and inelastic scattering of electrons of the sample as shown in **Figure 2.14**. The objective lens focuses the scattered and transmitted electron wave function from the same lattice points of the sample to the image plane. The intensity distribution of the interference pattern formed by the electron wave is used to record the TEM image of the sample [173].

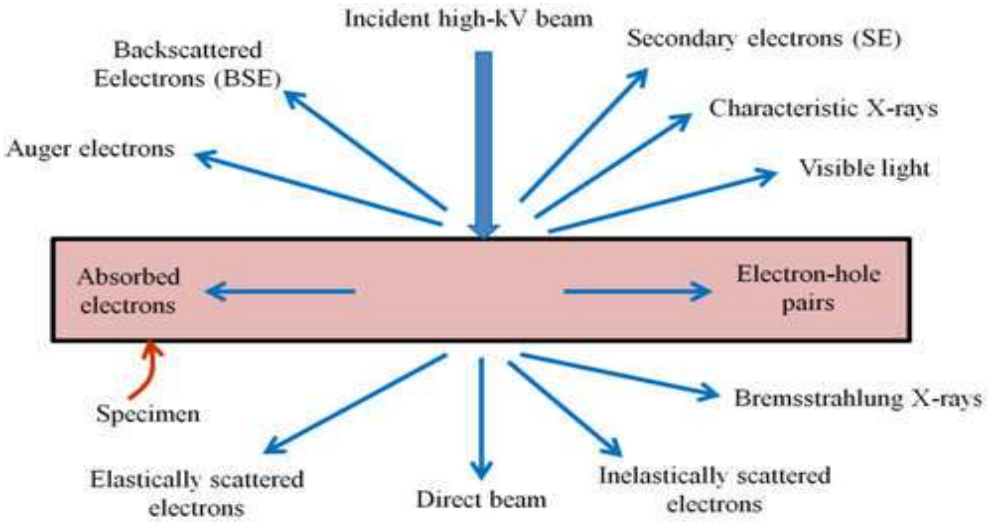

Figure 2.14 Interaction of electron beam with sample specimen

The image is formed on phosphor screen or charge coupled device camera. A schematic diagram of TEM operation is shown in **Figure 2.15**. TEM micrograph is a diffraction pattern of electron wave formed by the crystal lattice which are treated as Fourier transform of the lattice and an inverse Fourier transform of the micrograph. The TEM image is formed at the objective lens. The assembly of intermediate lenses magnified the image before finally appearing on the screen. TEM image can be taken in four conventional modes [166, 174]

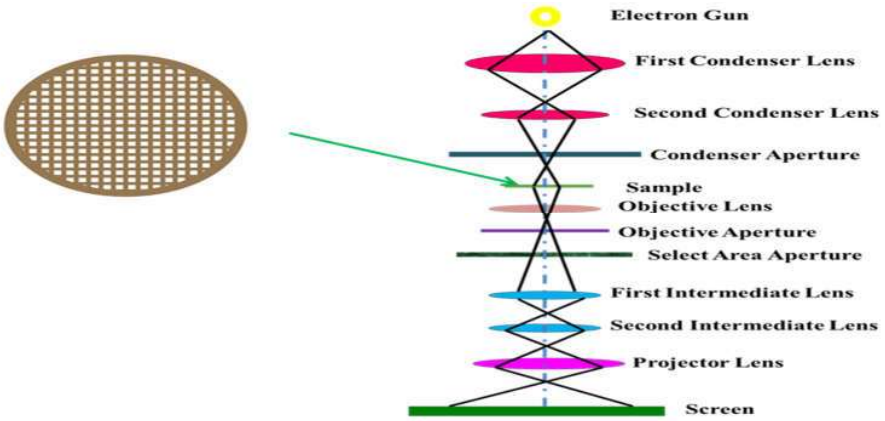

Figure 2.15 The Schematic view of a Transmission Electron Microscope (TEM).

. These are given below:

I. **Bright Field:** In this mode, the objective lens can be positioned at a particular position in the back focal plane. A bright field image is formed when the objective lens is positioned to allow the passing of a transmitted electron only. The image is made on the image plane of the objective lens.

II. **Dark Field:** In this mode, the objective lens allows passing of the diffracted electron beam only. Dark field image is formed by the scattered or diffracted electron.

III. **Diffraction contrast:** A contrast in the diffraction pattern or the "diffraction contrast" forms due to the variation in intensities of the diffracted electron beam coming from different areas of the sample. The resolution of the image is objective aperture-dependent and can be as low as 1 nm. This mode is used for observing defects and dislocations present in sample. This feature becomes distinct by inserting an objective aperture in the electron beam.

IV. **Selected Area Electron Diffraction (SAED):** In this mode, an intermediate aperture is inserted in the image plane of the objective lens which confines the electron beam to a particular or selected area of the sample. The sample is examined in the image mode until an area of interest is found. Then the mode is switched to diffraction mode and SAED pattern is taken.

High resolution mode in electron microscope offers direct imaging of critical details of the atomic structure of the sample. HRTEM directly shows the two-dimensional projection of the crystal with defects and dislocations. In HRTEM imaging a thin slice of the sample is tilted in such a way that the electron beam becomes perpendicular to the lattice direction. These lattice planes diffract electron beams according to Bragg's law. The objective lens focuses the diffracted beams and primary beam, and their interference pattern leads to an enlarged picture

of the periodic lattice fringes. The picture is magnified 106 times and brought to the final screen. The contrast present in the images is related with diffraction of electron waves itself. Spherical aberration, astigmatism limits, the limit of resolution and clarity limit of a HRTEM is minimized differently. HRTEM is also used for high resolution study of nano-materials at the atomic scale. By the use of new and sophisticated technique, it is possible to get an image down to "resolution limit" [173]. In this work, the measurement has been performed by FEI, Tecnai G2 20 Twin Type operated at 200 kV [**Figure 2.16(a) - (b)**]. The morphology view of the prepared nano composition obtained from HRTEM study [**Figure 2.16 (c)**].

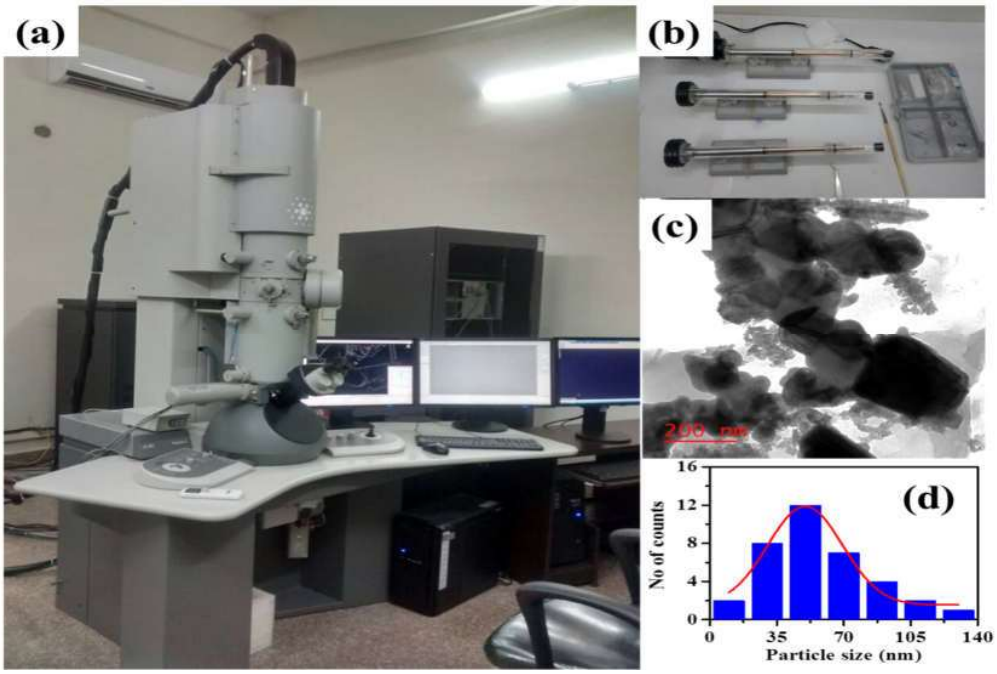

Figure 2.16 (a) TEM facility at IIT-BHU **(b)** TEM grid for measurement **(c)** HR-TEM image of sample **(d)** Distribution function for spherical grains.

The following approach has been adopted to determine the average particle size. The size distribution histogram of spherical nanoparticles is fitted with Gaussian distribution function as described by **Eq. (2.21)** [175] is shown in **Figure 2.16 (d)**.

$$y = y_o + \frac{Ae^{\frac{-4\ln(2)(x-x_c)^2}{w^2}}}{w\sqrt{\frac{\pi}{4\ln 2}}} \quad (2.22)$$

Where x_c is the diameter of spherical nano particle and $\frac{w}{2}$ is the least error in determination of particle size. Average size of the nano particles are determined by Gaussian fitting to the histogram (generated for distribution of particle size).

2.2.6.2 Field Emission Scanning Electron Microscope (FESEM)

A field emission cathode in electron gun of a scanning electron microscope provides a narrower beam at low as well as high electron energy, resulting in both improved spatial resolution and minimized sample charging and damage [176]. The electrons were generated by a field gradient in the presence of vacuum, then the beam passes through electromagnetic lenses was focused onto the specimen which results generation of various types of electrons through this interaction as shown in **Figure 2.17**. A detector ascertained the secondary electron and an image of the surface sample are formed by comparing the intensities of secondary electrons to the primary electron beam. Finally, the image is displayed on monitor equipped with the FESEM. FESEM produces clear, less electrostatically distorted images of spatial resolution to 50 nm, which is 10 to 100 times better than conventional SEM. The FE-SEM images of the investigated samples in this thesis work have been recorded by Nova Nano SEM 450 as shown in **Figure 2.17**.

Figure 2.17 FESEM facilities, IIT (BHU).

1.1.1.1 Energy dispersive X-ray spectroscopy (EDX)

The non-destructive Energy Dispersive X-ray analysis commonly known as EDX or Energy dispersive spectroscopy analysis (EDS) is an X-ray analysis to identify the elemental composition of materials of 0.5 to 1 atomic percent sensitivity. This facility is generally attached with electron microscopy instrument (SEM, TEM) where a specimen of interest is identified by the impact of a high energy electron beam and ejected electrons from inner shell of atomic orbitals of elements present in the sample. The resulting vacancy of the inner shell is filled by the electrons available in shell close to the vacant shell; these transitions are emitted as X-rays. Thus the information corresponding to the elements of the samples can be analyzed on the basis of energy of emitted X-ray. EDX gave qualitative, semi-quantitative information about the elements present in the composition. In the present thesis work, the elemental compositions of the prepared samples were confirmed from energy-dispersive X-ray analysis using EDXA spectrometer of model: Team Pegasus integrated EDS-EBSD with Octane Plus and Hikari Pro, as shown in **Figure 2.17** attached with FESEM/ Nova Nano SEM 450.

2.2.6.3 X-Ray Photoelectron Spectroscopy (XPS)

XPS is a non-destructive chemical surface analysis system that can be used to analyse the surface chemistry of materials in its as received state, or after some treatment such as; fracturing, cutting or scraping in air or UHV to explore bulk chemistry [176]. It provides the information about the presence of elements in compositions of the parts per thousand range, empirical formula; chemical state and electronic state of the elements that exist within a material. In XPS spectra measurement process, the X-rays are incident on the sample and simultaneous measurement between kinetic energy and numbers of electrons ejected from the top surface of the materials (1 to 10 nm) is shown in **Figure 2.18 (a)**. XPS spectra have been

recorded in high vacuum (P ≈ 10^{-8} milibar) or ultra-high vacuum (UHV ≈ 10^{-9} milibar) conditions, although a current area of development is an ambient pressure XPS, in which samples are analyzed at various pressure of few milibar. Ion beam etching process is used to clean off the surface contamination to get more extensive and accurate analysis in-depth profiling of elements. It also exposed in the heat to study the changes occurring by heating in the chemical composition and valence states of elements. Similarly, in the exposure of reactive gases, solutions, ion beam implantation, ultra-violet light, the XPS measurement has been carried out. It is routinely used to analyse inorganic compounds, metal alloys, semiconductors, polymers, elements, catalysts, glasses, ceramics, paints, papers, inks, woods, plant parts, teeth, bones, medical implants, bio-materials, ion-modified materials, and many others. XPS is also known as ESCA (Electron Spectroscopy for Chemical Analysis). In present thesis work, the XPS spectra of the samples have been recorded by PHI 5000 Versa Probe II spectrometer with the pressure of 5 x 10^{-11} Torr as shown in **Figure 2.18(b)**.

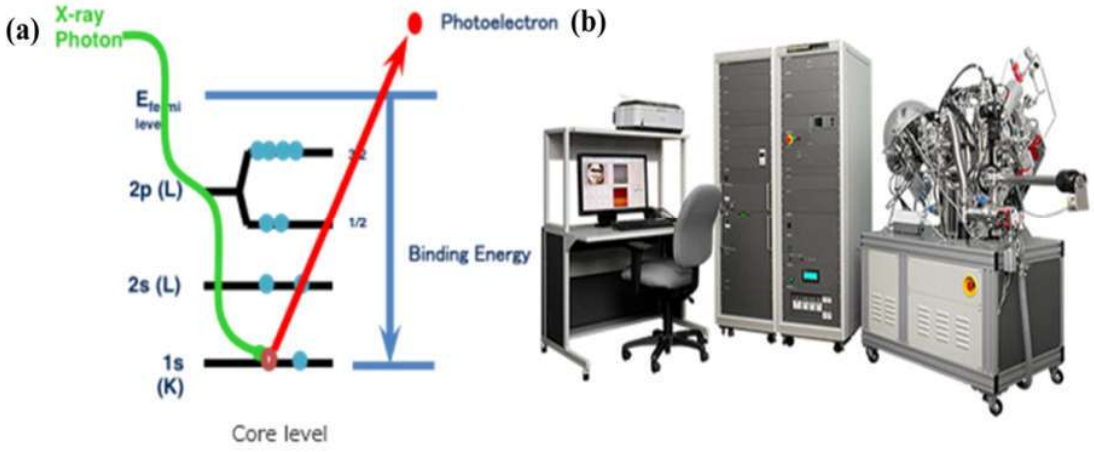

Figure 2.18 (a) Mechanism of X-ray Photoelectron Spectroscopy **(b)** Experimental set-up for XPS measurement.

2.2.7 Optical Characterization Technique

2.2.7.1 Ultra-Violet Visible (UV-Vis) Spectroscopy

The UV-Vis spectroscopy has been used to study the absorption and reflectance of sample in the ultraviolet to visible spectral region. Further, the optical band gaps of the sample have been calculated from the UV-Vis data. The absorption or reflectance in the visible range directly affects the perceived colour of the chemicals involved. In this region of electromagnetic spectrum, the molecules undergo an electronic transition. It measures the intensity of light before it passes through the sample (I) and compares it to the intensity of light after it passes through the sample (I_o). The ratio (I/I_o) is called as transmittance expressed in percentage (%T). However, the absorbance (A) is defined in terms of transmittance as follows;

$$A = -\log\left(\frac{T}{100}\right)$$

The UV-Vis spectrometer can also be used to measure reflectance. In case of reflectance mode, the spectrometer measures the intensity of light reflected from sample (I) to the intensity of light reflected from a reference material (I_o) (such as a white tile). The ratio (I/I_o) is called as reflectance expressed in percentage (%R).

The spectrophotometer has four main components named as (i) light source (ii) sample holder (iii) diffraction grating of monochromator (iv) detector. The radiation source is operated in continuous mode for the visible wavelengths. The photomultiplier tube, a photodiode or charge-coupled device (CCD) is used as a detector. Single photodiode detectors and photomultiplier tube are used for scanning monochromator, which filters all wavelength and pass only single wavelength to detector at one time. The scanning monochromator moves the diffraction grating to "Step-through" each wavelength so that its intensity has been measured as a function of wavelength. UV-Vis spectrophotometer (Shimandzu, UV-2600) shown in **Figure 2.19** is used for present investigating sample.

Figure 2.19 Experimental Set-up for UV-Vis measurement (IIT BHU).

The optical band gap of the samples was determined by using well studied relation known as Tauc equation [177]. According to Tauc relation, the optical absorption strength depends on the difference between the photon energy and the band gap as follows:

$$(\alpha h\nu) = A(h\nu - E_g)^n \tag{2.23}$$

Where, h is Planck's constant, ν is the Photon's frequency, α is absorption coefficient,E_g is the band gap and A is proportionality constant. The value of exponent n denotes the nature of the electronic transition, whether allowed or forbidden and direct or indirect: for direct allowed transition n=1/2, for direct forbidden transition n=3/2, for indirect allowed transition n=2 and for indirect forbidden transition n=3 [178]. The band gap corresponding to direct transition was obtained by extrapolating the linear portion of $(\alpha h\nu)^2$ verses $h\nu$ curves such that $(\alpha h\nu)^2 = 0$. The typical plot of $(\alpha h\nu)^2$ vs. $h\nu$ is shown in **Figure 2.20**.

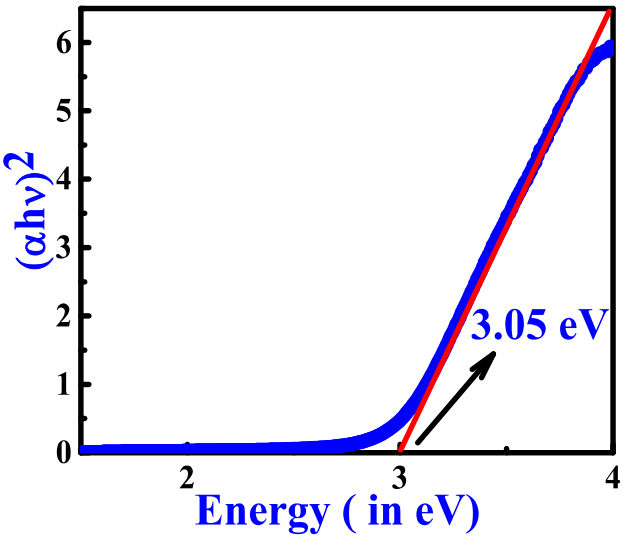

Figure 2.20 Tauc plot generated by Eq. 2.23.

2.2.7.2 Photoluminescence (PL) Spectroscopy

Photoluminescence spectroscopy (PL) is a powerful technique to study the optical property of a material. In this process, a substance absorbs photons (electromagnetic radiation) and then re-radiates photons. In other words, this process describes an excitation to a higher energy state and then return to allowed energy state accompanied by the emission of a photon. This process of light emission is known as luminescence. The time between absorption and emission is minimal. The quantum mechanics postulates are used to determine the selection rules between states. A fundamental principle can be used to understand and study the electronic configuration of simple atoms and molecules [179].

Photoluminescence is an essential method for measuring the purity and crystalline quality of semiconductors. The schematic diagram of a general purpose spectrophotometer is shown in **Figure 2.21 (a)**. This spectrophotometer exhibits a xenon lamp which used as excitation source. This lamp consists of high intensities of all wavelengths. Photoluminescence spectrophotometer is equipped with a monochromator to select single wavelength used in both

process. The monochromator used in excitation contains two gratings, which decreases stray light, i.e., light with different wavelengths from chosen one. Also, the monochromator use concave gratings, produced by holographic means to decrease stray light. Both monochromator are motorized to allow automatic scanning of wavelength. The fluorescence is detected with photomultiplier tubes and multiplies with the appropriate electronic devices. The output is usually presented in graphical form and stored digitally. The setup of Photoluminescence spectrophotometer (Horiba, Japan) is shown in **Figure 2.21 (b)** was used to collect using photoluminescence spectra using Xe (xenon) lamp as an excitation source.

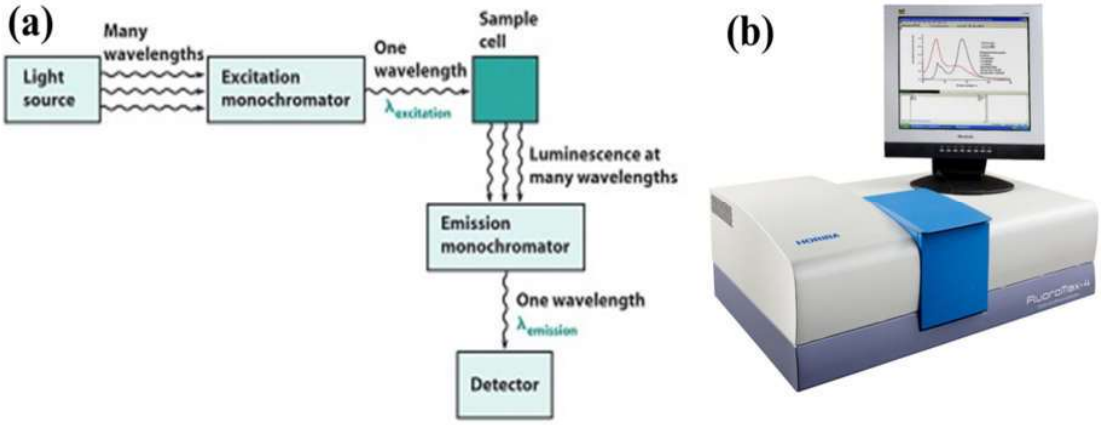

Figure 2.21 (a) Principle of photoluminescence spectroscopy **(b)** Experimental set-up used in the present investigation.

2.2.8 Alternating current (AC) Electrical data analysis

To characterize the electrical property of a material, electrochemical impedance spectroscopy (EIS) technique has been used. On applying an alternating voltage or current to experimental sample, the impedance, conductivity, dielectric property and modulus spectroscopic analysis of the samples are observed against ac signal.

For the electrical properties measurement, the necessary electrode was created on both the surfaces of pellets using a high temperature silver paste (Alfa Aesar). The silver coated pellets were then heated upto 500^{o}C for 30 min to form proper electrode. The electrical response of the different samples was carried out in the presence of ac signal by mounting the pellet in a sample holder inside a tube furnace in an air atmosphere using two probe methods. The experimental set up used for electrical measurement under this investigation has been shown in **Figure 2.22**. The frequency and temperature dependence of different electrical responses such as impedance, dielectric constant, dielectric loss, complex modulus, etc., were measured with the help of an LCR meter (Agilent E-4980, USA) interface with a PC in the frequency range 20 Hz- 2MHz and in temperature range 60^{o}C to 600^{o}C

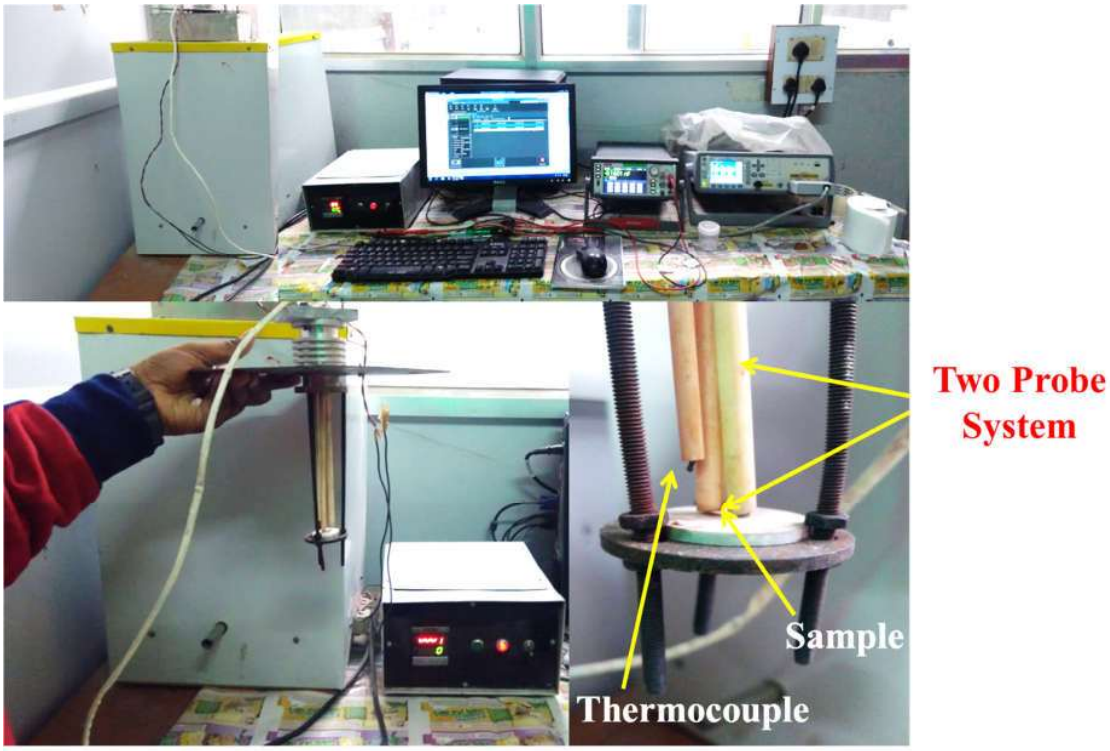

Figure 2.22 Experimental Set-up used for Electrical Characterization of sample (IIT BHU).

With the help of these studies, the ion dynamics and relaxation phenomenon, etc. were understood. Two parameters capacitance (C) and dissipation factor (D) were calculated within same frequency and temperature range. Further, using these parameters following parameters were calculated;

Dielectric constant $(\varepsilon_r) = \frac{C*d}{\varepsilon_o*A}$

Conductance $(G) = \omega * C * D$

Conductivity $(\sigma) = G * \left(\frac{d}{A}\right)$

Real part of impedance $(Z') = \frac{D^2}{G*(1+D^2)}$

Imaginary Part of impedance $(Z'') = \frac{Z'}{D}$

Real Part of modulus $(M') = \omega * C_o * Z''$

Imaginary Part of modulus $(M'') = \omega * C_o * Z'$

Where, d, A and C_o are the thickness, crossectional area of pellet and capacitance of free space respectively. The capacitance of free space was calculated by formula $C_o = \frac{\varepsilon_o*A}{d}$ and $\omega = 2\pi f$. After calculating these parameters, the detailed study of different spectroscopic analysis has been carried out depending on properties of materials. The $Z^*(\omega)$ can be represented by following equation in complex plane;

$$Z^*(\omega) = Z'(\omega) - iZ''(\omega) \quad (2.24)$$

Where, $Z'(\omega)$ and $Z''(\omega)$ are the real and imaginary part of the impedance respectively, which are measured simultaneously as a function frequency and $i = \sqrt{-1}$. The frequency dependent complex impedance data of a material can also represented in terms of other complex parameters like complex admittance (Y^*), complex modulus (M^*), complex permittivity (ε^*) and dielectric loss tangent $(\tan\delta)$. These frequency dependent parameters are related to each other by the following relation;

$$Z^* = Z' - iZ'' = \frac{1}{i\omega_o C_o \varepsilon^*(\omega)} \quad (2.25)$$

$$Y^* = Y' - iY'' = (i\omega_o C_o \varepsilon^*) \quad (2.26)$$

$$\varepsilon^* = \varepsilon' - i\varepsilon'' \quad (2.27)$$

$$M^* = M' - iM'' = \frac{1}{\varepsilon^*(\omega)} = i\omega C_o Z^*(\omega) \quad (2.28)$$

$$\tan(\delta) = \frac{\varepsilon''}{\varepsilon'} = \frac{M'}{M''} = \frac{Y''}{Y'} = \frac{Z''}{Z'} \quad (2.29)$$

Where C_o is the geometrical capacitance, $Z'(\omega)$, $Y'(\omega)$, $\varepsilon'(\omega)$, $M'(\omega)$ and $Z''(\omega)$, $Y''(\omega)$, $\varepsilon''(\omega)$, $M''(\omega)$ denote the frequency dependent real and imaginary components of the impedance, admittance, permittivity and modulus respectively.

2.2.8.1 Complex Impedance Spectroscopy Analysis

Overall dielectric and electrical properties of polycrystalline electronic ceramics have contributions from (i) bulk or grains (ii) grain boundaries and (iii) electrode specimen interface or electrode polarization. Impedance analysis emerged as a powerful and simple tool to separate out these contributions [180]. Two types of plots can be generated to study the ion dynamics and relaxation mechanism involved in the ceramics: **(1)** Complex plane plots, e.g., Z'' vs. Z' and M'' vs. M' plots and **(2)** Spectroscopic plots Z''/Z' or M''/M' vs. $\log f$ plots. If a polycrystalline ceramic has contributions of grains, grain boundaries and electrode, then each of these contributions can be represented by a circuit element containing R and C connected in parallel. The sample can therefore be represented by an equivalent circuit containing three parallel RC circuit elements connected in series as shown in **Figure 2.23**. Cole-Cole plot (Nyquist plot) is the most widely used to investigate frequency response information of a system by complex impedance function $Z^* = Z'(\omega) - iZ''(\omega)$, where $Z'(\omega)$ and $Z''(\omega)$ are the real and imaginary parts of $Z^*(\omega)$. The real Z' and imaginary Z'' for the equivalent circuit as shown in **Figure 2.23** can be determined as;

$$Z' = \frac{R_g}{(1+\omega R_g C_g)^2} + \frac{R_{gb}}{(1+\omega R_{gb} C_{gb})^2} \quad (2.30)$$

$$Z'' = R_g \frac{\omega R_g C_{gb}}{(1+\omega R_g C_g)^2} + R_{gb} \frac{\omega R_{gb} C_{gb}}{(1+\omega R_{gb} C_{gb})^2} \quad (2.31)$$

Where, R_g and C_g are the bulk (grain) resistance and capacitance, respectively, and R_{gb} and C_{gb} are the corresponding quantities for the interfacial boundary (grain boundary). It is possible to identify the relative position of the two arcs in a complex plane by frequency. The bulk arc generally lies at a higher frequency than the interfacial boundary, as the interfacial boundary relaxation time is much larger than the bulk crystal. In a complex plane impedance analysis, three semi-circular arcs with their center on the actual axis are observed if each of the above three contributions has a single relaxation time value as shown in **Figure 2.23**. Relaxation time (τ) which is equal to the inverse of the angular frequency, (ω) at which the relaxation peak occurs, is given by the product of RC i.e.

$$\tau = 1/\omega = RC \quad (2.32)$$

Since the arc of bulk (grain) may be masked in the limited frequency range. R_g, R_{gb} and R_{el} represent the resistive contributions of grains, grain boundaries and electrode polarization process and by using **Eq. (2.34)**, the C_g, C_{gb} and C_{el} can be easily calculated.

Hirose and West give the equations for the real axis intercepts for various Emittance functions in complex plane plots. The intercepts of the arcs with the real axis (Z') give the resistive contributions $\boldsymbol{R_g}$, R_{gb} and $\boldsymbol{R_{el}}$ in the impedance plots.

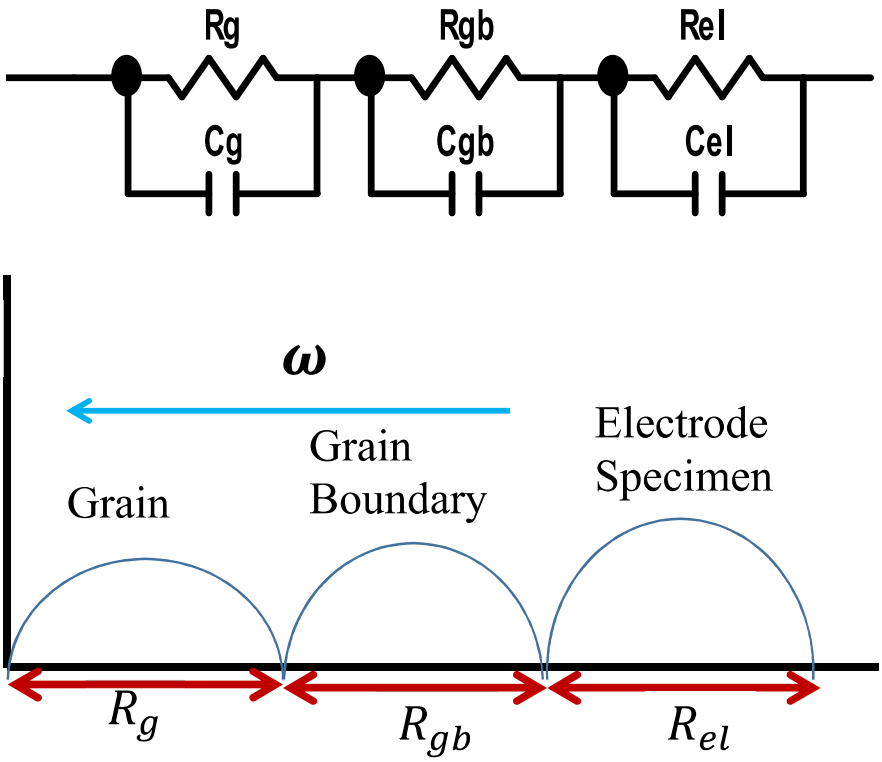

Figure 2.23 Equivalent circuit for polycrystalline ceramic sample and their frequency response in complex Impedance plot.

2.2.8.2 Complex Modulus Spectroscopy Analysis

Complex Impedance Spectroscopy (CIS) is a helpful characterization technique to understand the effect of grain boundaries in ceramic materials. To differentiating grain-boundary conduction process from the electrode polarization effect, the complex modulus formalism is extensively studied. It is also used to identify and understand bulk properties, electrical conductivity and relaxation time [181]. Therefore, this formalism provides information related to electrical process involved in the materials and to understand the same as a function of frequency at different temperatures [182]. The inhomogeneous nature of polycrystalline sample due to the effect of bulk and grain boundary that cannot be distinguished from impedance plots can also be determined with precision. The other main benefits of

modulus formalism are that it effectively suppresses the electrode effect. Because of the aforesaid reasons, complex modulus formalism has been used.

The Nyquist plot was obtained using modulus data similar to impedance is shown in **Figure 2.24**. The intercepts on M' axis in modulus plots are inversely proportional to the different capacitive contributions (C_o/C_g, C_o/C_{gb} and C_o/C_{el}). The most sluggish processes of electrode polarization seem in the lowest frequency range followed by grain boundaries in the intermediate frequency range and the contribution of bulk or grain appears in the impedance plots at the highest frequency range. Frequency increases in the opposite direction in complex plane impedance and modulus plots. The value of the capacitance from the impedance plots and resistance from the modulus plots can be obtained from the frequency of the peak point in the arc where the relation $\omega RC = 1$ is satisfied. If any of the above contributions has a distribution of relaxation times rather than a single value, then one observes a depressed circular arc with its center below the Z' or M' axis.

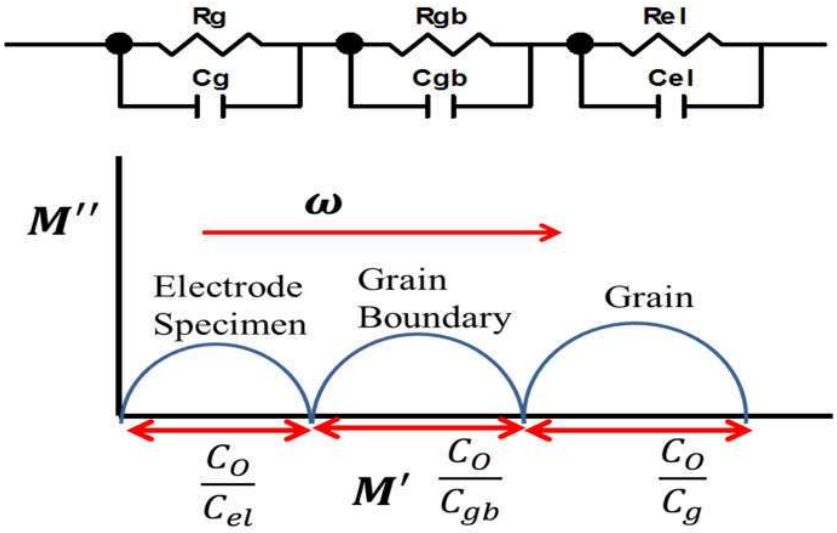

Figure 2.24 Equivalent circuit for polycrystalline ceramic sample and corresponding frequency response in the complex Modulus plots.

The actual number of arcs appearing in the complex plane plots also depends on the ratio of various times constants. An electronic ceramic is having a negligible value of electrode-specimen interface contribution (ohmic contact); can be represented by two parallel RC elements connected in series. These resistances and capacitances (i.e., R_g, R_{gb}, C_g and C_{gb}) can be estimated from the best fit of the Cole-Cole plots at various temperatures from modulus data also. Whether a full, partial or no semi-circle is observed in a Cole-Cole plot, depends on the strength of relaxation, the value of distribution parameters is determined by employing fitting of **Eq. (2.29)** and **(2.30)**.

2.2.8.3 Conductivity Spectroscopy analysis

Electrical conductivity spectroscopy is a most powerful technique for the investigation of electrochemical properties. The ion dynamics need to be understood to tailor the material properties. The various research groups and authors have therefore tried different approaches to understanding the ion dynamics of glasses, polymers, semiconductors, nano-composites, and poly-crystals, etc. [183]. In the former description, the real part of ac conductivity, σ' could be described in term of Johnscher's power law as shown in **Figure 2.25** [184, 185];

$$\sigma = \sigma_{dc}\left[1 + \left(\frac{f}{f_H}\right)^n\right] \tag{2.33}$$

The above expression consists of two parts: (i) frequency independent part commonly known as dc conductivity, σ_{dc} caused by the random motion of the mobile charge carriers and (ii) frequency dependent ac component f_H is the cross over frequency from dc to the dispersive conductivity region caused by the hopping motion of the charge carriers in grains and grain boundaries and n is power exponent represent the electric relaxation behaviour of the material with value generally smaller than unity. Almond and West proposed crossover frequency as

the hopping frequency in their work [186]. The hopping frequency, $\boldsymbol{f_H}$, can be correlated with dc conductivity through Nernst-Einstein relation.

$$\sigma_{dc} = en_c\mu = \frac{n_c e^2 \gamma \lambda^2}{kT} f_H \tag{2.34}$$

Where, n_c is the concentration of the mobile charge carriers, μ is their mobility, e is the electronic charge, γ is a geometrical factor for ion hopping, λ is the hopping distance, and k is Boltzmann's constant. The above equation can be used to estimate the charge carrier concentration and its variation with temperature. It has been proven that conductivity spectra of electronic/ionic conducting materials at different temperature follow the scaling law known as the time-temperature superposition principle (TTSP). The conductivity isotherm can be superimposed on a single master curve, which is mathematically expressed as [187].

$$\frac{\sigma}{\sigma_{dc}} = F\left(\frac{f}{f_H}\right) \tag{2.35}$$

Where F is a temperature independent function and f_H is a temperature dependent scaling parameter. In the literature various types of scaling models have been proposed by different workers such as Summerfield scaling [188], Roling et al. scaling [55], Sidebottom scaling [189], Baranovskii and Cordes scaling [190] and Ghosh scaling [187]. All models differ according to the selection of scaling parameter i.e., hopping frequency f_H. In Summerfield scaling hopping frequency defined as $f_H = \sigma_{dc}.T$, in Roling et al. scaling $f_H = \sigma_{dc}.T/x$ and in Ghosh scaling chosen f_H as the scaling parameter. Among the above scaling, Ghosh scaling is widely applicable because of automatic consideration of changes in permittivity and the Haven ratio [187].

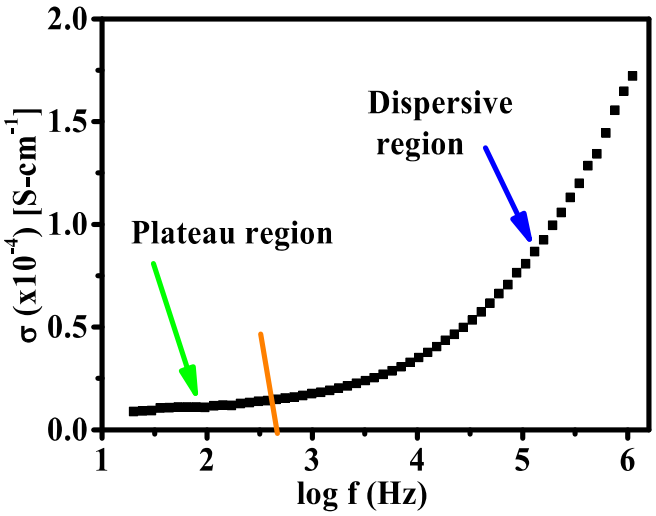

Figure 2.25 Conductivity spectra of a polycrystalline material.